

Black-box superconducting circuit quantization

Simon E. Nigg, Hanhee Paik, Brian Vlastakis, Gerhard Kirchmair, Shyam Shankar,
Luigi Frunzio, Michel Devoret, Robert Schoelkopf and Steven Girvin
Departments of Physics and Applied Physics, Yale University, New Haven, CT 06520, USA
(Dated: April 4, 2012)

We present a semi-classical method for determining the effective low-energy quantum Hamiltonian of weakly anharmonic superconducting circuits containing mesoscopic Josephson junctions coupled to electromagnetic environments made of an arbitrary combination of distributed and lumped elements. A convenient basis, capturing the multi-mode physics, is given by the quantized eigenmodes of the linearized circuit and is fully determined by a classical linear response function. The method is used to calculate numerically the low-energy spectrum of a 3D-transmon system, and quantitative agreement with measurements is found.

PACS numbers: 42.50.Ct,85.25.Am,42.50.Pq,03.67.-a

Superconducting electronic circuits containing nonlinear elements such as Josephson junctions (JJs) are of interest for quantum information processing [1, 2], due to their nonlinearity and weak intrinsic dissipation. The discrete low-energy spectrum of such circuits can now be measured to a precision of better than one part per million [3]. The question thus naturally arises of how well one can theoretically model such man-made artificial atoms. Indeed, increasing evidence indicates that due to increased coupling strengths [4], current models are reaching their limits [5–9] and in order to further our ability to design, optimize and manipulate these systems, developing models beyond these limits becomes necessary. This is the goal of the present work.

An isolated ideal JJ has only one collective degree of freedom: the order parameter phase difference φ across the junction. The zero-temperature, sub-gap physics of this system, with Josephson energy E_J and charging energy E_C , is described by the Cooper-pair box Hamiltonian

$$H_{\text{CPB}} = 4E_C(\hat{N} - N_g)^2 - E_J \cos(\hat{\varphi}), \quad (1)$$

where \hat{N} is the Cooper-pair number operator conjugate to $\hat{\varphi}$ and N_g an offset charge. This model is exactly solvable in terms of Mathieu functions [10, 11]. The crucial feature that emerges from this solution is that the charge dispersion, i.e. the maximal variation of the eigenenergies with N_g , is *exponentially* suppressed with E_J/E_C while the relative anharmonicity decreases only algebraically with a slow power-law in E_J/E_C . As a consequence, there exists a regime with $E_J \gg E_C$ – the transmon regime – where the anharmonicity is much larger than the linewidth (e.g. due to fluctuation of the offset charge N_g), thus satisfying the operability condition of a qubit [12]. This is the regime of interest here.

In order to be useful for quantum information processing tasks, several Josephson qubits must be made to controllably interact with each other and spurious interactions with uncontrolled (environmental) degrees of freedom must be minimized. In circuit quantum elec-

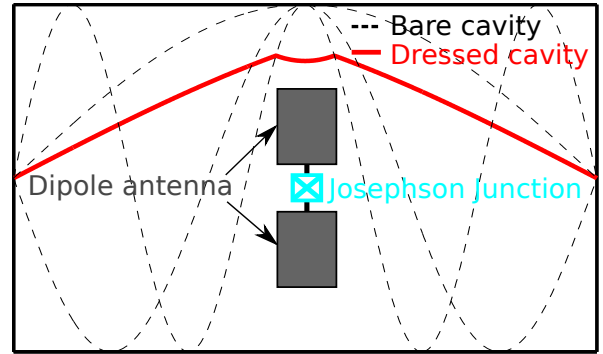


FIG. 1. (Color online) Cartoon of a JJ at the center of a broadband dipole antenna inside a 3D microwave cavity. The presence of the antenna alters the geometry of the cavity-mode (full (red) curve) and a precise description requires the inclusion of many bare modes (dashed curves).

trodynamics [2, 11, 13] (cQED), this is achieved by coupling the JJs to a common microwave environment with a desired discrete mode structure. So far such systems have mostly been described theoretically by models well known from quantum optics such as the single-mode Jaynes-Cummings model and extensions thereof [14].

When applied to superconducting circuits with multi-level artificial atoms, multi-mode cavities and increased coupling strengths [4, 6, 7] however, several technical and practical difficulties with these approaches arise. For example, capturing important effects of non-computational qubit states requires going to high orders in perturbation theory [15]. Also, determining the *bare* Hamiltonian parameters, in terms of which these models are defined, is cumbersome and requires iterating between experiment and theory. Perhaps even more important are the shortcomings of the traditional approaches in dealing with the multiple modes of the cavity. Indeed high-energy, off-resonant cavity modes have already been measured to contribute substantially to the inter-qubit interaction strength [8, 15] and, via the multi-mode Purcell effect,

also to affect the coherence properties (relaxation and dephasing) of the qubits [5]. Attempts at including this multi-mode physics in the standard models however, lead to difficulties with diverging series and QED renormalization issues [8, 16], which to the best of our knowledge remain unresolved. Fig. 1 illustrates the origin of the problem with the example of a JJ inside a 3D cavity (3D-transmon) [3]. The presence of a relatively large metallic dipole antenna [17] can strongly alter the geometry of the cavity modes. This essentially classical effect, can be accounted for precisely only by including a sufficiently large number of bare modes.

In contrast, we propose to start by considering the coupled but *linearized* problem in order to find a basis that incorporates the main effects of the coupling between multi-level qubits and a multi-mode cavity and then account for the weak anharmonicity of the Josephson potential perturbatively. The crucial assumption made here is that charge dispersion effects can be safely neglected. This is reasonable given that in state-of-the-art implementations of transmon qubits [3, 18], charge dispersion only contributes a negligible amount to the measured linewidths. Previous work discussed the nonlinear dynamics of a JJ embedded in an external circuit classically [19]. Here we go one step further and show how the knowledge of a classical, in principle measurable, linear response function lets us quantize the circuit, treating qubits and cavity on equal footing.

Single junction case. We consider a system with a JJ with *bare* Josephson energy E_J and charging energy E_C , in parallel with a linear but otherwise arbitrary electromagnetic environment as depicted in Fig. 2 (a). Neglecting dissipation, the unbiased junction alone is described by the Hamiltonian (1). At low energies, when $E_J \gg E_C$, quantum fluctuations of the phase φ across the junction are small compared with π and, as emphasized in the introduction, the probability of quantum tunneling of the phase between minima of the cosine potential is negligibly small. It is then reasonable to expand the latter in powers of φ , thus obtaining the approximate circuit representation of Fig. 2 (b), in which the spider symbol [19] represents the purely nonlinear part and $L_J = \phi_0^2/E_J$ and $C_J = e^2/(2E_C)$ the linear parts of the Josephson element. Here $\phi_0 = \hbar/(2e)$ is the reduced flux quantum. To leading order, the energy of the spider element is given by $E_{\text{nl}} = -\phi_0^2 \varphi^4/(24L_J)$.

A quantity of central importance in the following is the impedance $Z(\omega)$ of the linear part of the circuit depicted in Fig. 2 (c). The latter is a complex meromorphic function and by virtue of Foster's theorem [20, 21] can be synthesized by the equivalent circuit of parallel LCR oscillators in series shown in Fig. 2 (d). Explicitly

$$Z(\omega) = \sum_{p=1}^M \left(j\omega C_p + \frac{1}{j\omega L_p} + \frac{1}{R_p} \right)^{-1}, \quad (2)$$

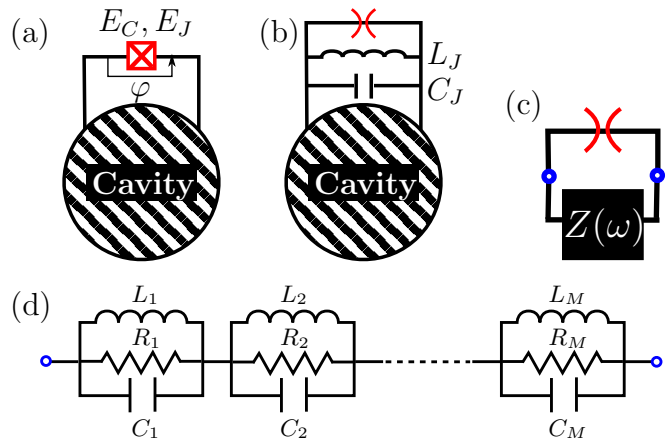


FIG. 2. (Color online) (a) Schematics of a JJ (red boxed cross) coupled to an arbitrary linear circuit (striped disk). (b) The Josephson element is replaced by a parallel combination of: a linear inductance L_J , a linear capacitance C_J and a purely nonlinear element with energy $E_J(1 - \cos(\varphi)) - (E_J/2)\varphi^2$, represented by the spider symbol. (c) The linear part of the circuit shown in (b) is lumped into an impedance $Z(\omega)$ seen by the nonlinear element. (d) Foster-equivalent circuit (pole-decomposition) of the impedance $Z(\omega)$.

where M is the number of modes [22] and we have adopted the electrical engineering convention of writing the imaginary unit as $j = -i$. This equivalent circuit mapping corresponds, in electrical engineering language, to diagonalizing the linearized system of coupled harmonic oscillators. The resonance frequencies of the linear circuit are determined by the real parts of the poles of Z or more conveniently by the real parts of the zeros of the admittance defined as $Y(\omega) = Z(\omega)^{-1}$, and for weak dissipation, i.e. $R_p \gg \sqrt{L_p/C_p}$, are given by $\omega_p = (L_p C_p)^{-\frac{1}{2}}$. The imaginary parts of the roots $(2R_p C_p)^{-1}$, give the resonances a finite width. The effective resistances are given by $R_p = 1/\text{Re}Y(\omega_p)$ and the effective capacitances are determined by the frequency derivative on resonance of the admittance as $C_p = (1/2)\text{Im}Y'(\omega_p)$. Here and in the following the prime stands for the derivative with respect to frequency. Note that $\text{Im}Y'(\omega) > 0$ [20]. Together this yields a compact expression for the quality factor of mode p :

$$Q_p = \frac{\omega_p \text{Im}Y'(\omega_p)}{2 \text{Re}Y(\omega_p)}. \quad (3)$$

When applied to the mode representing the qubit, Eq. (3) gives an estimate for the Purcell limit on the qubit lifetime $T_1 = Q_{\text{qb}}/\omega_{\text{qb}}$ due to photons leaking out of the cavity.

In order to derive the effective low-energy quantum Hamiltonian of the circuit, we next neglect dissipation ($R_p \rightarrow \infty$) and introduce the normal (flux) coordinates $\phi_p(t) = f_p e^{j\omega_p t} + (f_p)^* e^{-j\omega_p t}$ associated with each LC

oscillator in the equivalent circuit. We can then immediately write the classical Hamiltonian function of the equivalent circuit as $\mathcal{H}_0 = 2 \sum_{p=1}^M (f_p)^* (L_p)^{-1} f_p$, where the subscript 0 indicates that we consider the linear part of the circuit. Kirchhoff's voltage law implies that up to an arbitrary constant, $\phi(t) = \sum_{p=1}^M \phi_p(t)$, where $\phi(t) = \int_{-\infty}^t V(\tau) d\tau$ is the flux coordinate of the junction with voltage $V(t)$. Note that by the second Josephson relation, the order parameter phase difference is related to the latter via $\varphi(t) = \phi(t)/\phi_0$ (modulo 2π).

Quantization is achieved in the canonical way [23, 24] by replacing the flux amplitudes of the equivalent oscillators by operators as

$$f_p^{(*)} \rightarrow \sqrt{\frac{\hbar}{2}} \mathcal{Z}_p^{\text{eff}} a_p^{(\dagger)}, \quad \mathcal{Z}_p^{\text{eff}} = \frac{2}{\omega_p \text{Im} Y'(\omega_p)}, \quad (4)$$

with the dimensionless bosonic annihilation (creation) operators a_p (a_p^\dagger). Direct substitution yields the Hamiltonian $H_0 = \sum_p \hbar \omega_p a_p^\dagger a_p$ of M uncoupled harmonic oscillators (omitting the zero-point energies) and the Schrödinger operator of flux across the junction is

$$\hat{\phi} = \sum_{p=1}^M \sqrt{\frac{\hbar}{2}} \mathcal{Z}_p^{\text{eff}} (a_p + a_p^\dagger). \quad (5)$$

We emphasize that the harmonic modes a_p represent collective excitations of the linear circuit and their frequencies ω_p are the equivalent of dressed oscillator frequencies. The coupling in the linear circuit is treated exactly and in particular no rotating wave approximation is used.

The Hamiltonian of the circuit including the JJ is then $H = H_0 + H_{\text{nl}}$, where $H_{\text{nl}} = -(\hat{\phi})^4 / (24\phi_0^2 L_J) + \mathcal{O}((\hat{\phi}/\phi_0)^6)$. Physical insight may be gained by treating the nonlinear terms as a perturbation on top of H_0 assuming the eigenstates $|n_1, n_2, \dots, n_M\rangle$ of the latter with energies $E_{n_1, n_2, \dots, n_M}^{(0)} = \sum_i n_i \hbar \omega_i$, to be non-degenerate. Considering only the leading order ϕ^4 nonlinearity, one then obtains the reduced Hamiltonian

$$H_4 = H_0' + \frac{1}{2} \sum_{pp'} \chi_{pp'} \hat{n}_p \hat{n}_{p'}. \quad (6)$$

Here $\hat{n}_p = a_p^\dagger a_p$ and $H_0' = H_0 + \sum_p \Delta_p \hat{n}_p$ includes a correction to the Lamb-shift given by $\Delta_p = -\frac{e^2}{2L_J} \left(\mathcal{Z}_p^{\text{eff}} \sum_q \mathcal{Z}_q^{\text{eff}} - (\mathcal{Z}_p^{\text{eff}})^2 / 2 \right)$. We have further introduced the generalized χ -shift $\chi_{pp'}$ between modes p and p' . Clearly, $\alpha_p \equiv \chi_{pp}$ is the anharmonicity of the first excited state (self-Kerr) of mode p while $\chi_{pp'} = \chi_{p'p}$ with $p \neq p'$ is the state-dependent frequency shift per excitation (cross-Kerr) of mode p due to the presence of a single excitation in mode p' . Explicitly we find

$$\chi_{pp} = -\frac{L_p C_J}{L_J C_p} E_C, \quad \chi_{pp'} = -2\sqrt{\chi_{pp} \chi_{p'p'}}. \quad (7)$$

Note that all modes acquire some anharmonicity due to the presence of the nonlinear JJ. There is thus no strict separation of qubit and cavity anymore. Colloquially, a mode with strong (weak) anharmonicity will be called qubit-like (cavity-like). Interestingly, in this lowest order approximation, the anharmonicity of mode p is seen to be proportional to the inductive participation ratios [19] $i_p \equiv L_p/L_J$ and inversely proportional to the capacitive participation ratio $c_p \equiv C_p/C_J$. In the absence of a galvanic short of the junction in the resonator circuit, as is the case e.g. for a transmon qubit capacitively coupled to a cavity, it follows from the sum rule $\lim_{\omega \rightarrow 0} [Z(\omega)/(j\omega)] = \sum_p L_p = L_J$ that $i_p \leq 1$. Similarly, in the absence of any capacitance in series with C_J , it follows that $c_p \geq 1$, because $\lim_{\omega \rightarrow 0} [j\omega Z(\omega)] = \sum_p C_p^{-1} = C_\Sigma^{-1}$, where $C_\Sigma = C_J + C_\parallel$ and C_\parallel is the total capacitance in parallel with C_J . Hence we see that in this experimentally relevant case, the effective anharmonicity of the qubit-like mode is always reduced as compared with the anharmonicity of the bare qubit given by $-E_C$ [11]. Remarkably, in this approximation we find (see Eq. (7)) that the cross-Kerr shift between two modes is twice the geometric mean of the anharmonicities of the two modes.

We emphasize that the above expressions do not however account for higher order effects in anharmonicity such as the change of sign of the cross-Kerr shift observed in the straddling regime [11, 25]. Such effects are however fully captured by the full model $H = H_0 + H_{\text{nl}}$, which can be solved numerically. Remarkably, because the *dressed* modes already resum all the *bare* harmonic modes, typically only a few dressed modes $M^* \ll M$ need to be included for good convergence, thus considerably reducing the size of the effective Hilbert space, which scales as $\prod_{p=1}^{M^*} (N_p + 1)$ where N_p is the maximal allowed number of excitations in mode p (e.g. $N_p = 1$ in a two-level approximation).

Charge dispersion. By assumption charge dispersion effects are neglected in the above approach. One may however ask how the charge dispersion of an *isolated* JJ is affected when the latter is coupled to a cavity. As in the Caldeira-Leggett model [26], the coupling between the JJ and Harmonic oscillators suppresses the probability of flux tunneling and hence reduces charge dispersion of the qubit further. A simple estimate of the suppression factor is provided by the probability P_0 of leaving the circuit in the ground state after a flux tunneling event and is found to be given by the ‘‘Lamb-Mössbauer’’ factor $P_0 \approx e^{-\frac{1}{2} \sum_{p \neq \text{qb}} \left(\frac{\delta q_p^2}{2C_p} \right) / (\hbar \omega_p)}$, where the sum excludes the qubit mode and $\delta q = C_J \phi_0 / \tau$ is the charge (momentum) kick generated by a ϕ_0 flux slip through the JJ of duration τ and $C_p = (1/2) \text{Im} Y'(\omega_p)$. Thus our assumption of neglecting charge dispersion of the qubit is well justified.

Interestingly though, each eigenmode of the system inherits some charge dispersion. This effect, essentially a

ν_{01} (GHz)		ν_c (GHz)		ν_{02} (GHz)		α_{qb} (MHz)		χ (MHz)		L_J (nH)	C_J (ff)
7.77	(7.763)	8.102	(8.105)	15.33	(15.333)	-210	(-193)	-90	(-80.6)	5.83	7.6
7.544	(7.54)	8.126	(8.05)	14.808	(14.830)	-280	(-249)	-30	(-33.0)	6.12	9.2
7.376	(7.376)	7.858	(7.864)	14.489	(14.495)	-264	(-257)	-37.5	(-38.7)	6.67	4.0
7.058	(7.045)	8.005	(8.023)	13.788	(13.794)	-328	(-295)	-13.2	(-13.3)	7.45	5.2
6.808	(6.793)	8.019	(8.017)	13.286	(13.294)	-330	(-293)	-8	(-8.4)	7.71	7.8
6.384	(6.386)	7.832	(7.823)	12.45	(12.449)	-318	(-324)	-5.4	(-7.6)	9.40	0.34

TABLE I. Low-energy spectrum (ν_{01} , ν_c , ν_{02}), qubit anharmonicity (α_{qb}) and state-dependent cavity shift (χ) of six 3D-transmons. Results are shown in the format: experiment (theory). The theory values are obtained from a least square fit in C_J of the numerically computed lowest three energy levels of the ϕ^6 model. The fitted values of C_J are given in the last column. Their order of magnitude (a few femto-farads) agrees with estimates based on the sizes of the junctions. The Josephson inductances L_J are obtained from room-temperature resistance measurements of the junctions.

consequence of hybridization, is of particular importance for applications such as quantum information storage in high-Q cavities coupled to JJs and is the subject of work in progress.

Generalization to N junctions. The approach can be extended to circuits with multiple JJs connected in parallel to a common linear circuit. Details about the derivation are given in the supplementary material [27] and we here only state the results. For N qubits, the resonance frequencies of the linear part of the circuit are determined by the zeros of the admittance $Y_k(\omega) \equiv Z_{kk}(\omega)^{-1}$ for any choice of reference port $k = 1, \dots, N$, where \mathbf{Z} is the $N \times N$ impedance matrix of the linear part of the circuit with a port being associated with each junction. The flux operators of the N junctions, with reference port k , are given by ($l = 1, \dots, N$)

$$\hat{\phi}_l^{(k)} = \sum_{p=1}^M \frac{Z_{lk}(\omega_p)}{Z_{kk}(\omega_p)} \sqrt{\frac{\hbar}{2}} \mathcal{Z}_{kp}^{\text{eff}} (a_p + a_p^\dagger), \quad (8)$$

where $\mathcal{Z}_{kp}^{\text{eff}} = 2/[\omega_p \text{Im}Y_k'(\omega_p)]$. Note that the resonance frequencies are independent of the choice of reference port, while the eigenmodes do depend on it. In lowest order of PT and in the ϕ^4 approximation, we find

$$\alpha_p = -12\beta_{pppp}, \quad \chi_{qp} = -24\beta_{qqpp}, \quad q \neq p, \quad (9)$$

as well as the correction to the Lamb-shift $\Delta_p = 6\beta_{pppp} - 12\sum_q \beta_{qqpp}$. Here $\beta_{qq'pp'} = \sum_{s=1}^N \frac{e^2}{24L_J^{(s)}} \xi_{sq} \xi_{s q'} \xi_{sp} \xi_{s p'}$, and choosing the first port as the reference port ($k = 1$), $\xi_{sp} = \frac{Z_{s1}(\omega_p)}{Z_{11}(\omega_p)} \sqrt{\mathcal{Z}_{1p}^{\text{eff}}}$. Notice that the Cauchy-Schwarz inequality implies that $|\chi_{qp}| \leq 2\sqrt{\alpha_q \alpha_p}$. Also, if q and q' refer to two different qubit-like modes, then $\chi_{qq'}$ is a measure for the *total* interaction strength (cavity mediated and direct dipole-dipole coupling) between these two qubits.

Comparison with experiment. As a demonstration of this method, we apply it to the case illustrated in Fig. 1 of a single JJ coupled to a 3D cavity [3]. The admittance at the junction port Y is a parallel combination of the linearized qubit admittance and the admittance Y_c of the cavity-antenna system, i.e. $Y(\omega) =$

$j\omega C_J - j/(\omega L_J) + Y_c(\omega)$. The junction is assumed to be dissipationless corresponding to a Purcell-limited qubit and ohmic losses of the cavity are included in Y_c , which is complex. The Josephson inductance L_J is deduced from the measured junction resistance at room-temperature R_T , extrapolating it down to the operating temperature [28] of 15 mK and using the Ambegaokar-Baratoff relation, $E_J = \hbar\Delta/(8e^2 R_T)$. C_J – the only free parameter – is obtained by fitting the lowest three energy levels of the numerical solution of the ϕ^6 model to the measured spectrum [3]. Although Y_c may in principle be obtained from current-voltage measurements, this is not practical in this system, where the antenna is hard to access non-invasively, being inside a closed high-Q cavity. Instead we use a finite element High Frequency Simulation Software (HFSS) and obtain $Y_c(\omega)$ by solving the Maxwell equations numerically. Details on this simulation step are provided in the supplementary material [27].

From the zeros of the imaginary part of the admittance and their slopes we build and diagonalize the ϕ^6 Hamiltonian in a truncated Hilbert space, keeping in total three dressed modes (one qubit and two cavity modes) and allowing for maximally ten excitations per mode. The results of fitting the low-energy spectrum of six different samples are presented in Table I, where we also compare the predicted and measured qubit anharmonicities and χ -shifts. We find agreement with the measured spectrum at the sub-per cent level and to within ten per cent with the measured anharmonicities and χ -shifts.

Conclusion and outlook. We have presented a simple method to determine the effective low-energy Hamiltonian of a wide class of superconducting circuits containing lumped or distributed elements. This method is suitable for weakly nonlinear circuits, for which the normal modes of the linearized classical circuit provide a good basis in the quantum case. For an N qubit system it requires only the knowledge of an $N \times N$ (classical) impedance matrix. By working in a basis of dressed states, the parameters that appear in the Hamiltonian incorporate much of the renormalization induced by the coupling between a multi-level artificial atom and a multi-mode resonator. Consequently, the number

of free parameters is considerably reduced as compared with standard models based on the Jaynes-Cummings paradigm expressed in terms of the experimentally inaccessible bare parameters. We have demonstrated the usefulness of this method in designing superconducting quantum information processing units by computing the low-energy spectrum of a 3D-transmon. Finally, this model may represent a suitable starting point for future investigations of the emerging ultra-strong coupling regime of cQED.

Acknowledgments. We thank Claudia De Grandi, Eustace Edwards and Mazyar Mirrahimi for discussions and Mikhael Guy from the Yale HPC center for support with numerical simulations. SEN acknowledges financial support from the Swiss NSF. HP, GK, BV, LF, MD, RS and SG acknowledge financial support from IARPA, ARO (Contract W911NF-09-1-0514) and the American NSF (Contract DMR-1004406). All statements of fact, opinion or conclusions, contained herein are those of the authors and should not be construed as representing the official views or policies of IARPA, or the U.S. Government.

-
- [1] M. H. Devoret and J. M. Martinis, *Quantum Information Processing* **3**, 1 (2004).
- [2] A. Wallraff, D. I. Schuster, A. Blais, L. Frunzio, R.-S. Huang, J. Majer, S. Kumar, S. M. Girvin, and R. J. Schoelkopf, *Nature* **431**, 162 (2004).
- [3] H. Paik, D. I. Schuster, L. S. Bishop, G. Kirchmair, G. Catelani, A. P. Sears, B. R. Johnson, M. J. Reagor, L. Frunzio, L. I. Glazman, S. M. Girvin, M. H. Devoret, and R. J. Schoelkopf, *Phys. Rev. Lett.* **107**, 240501 (2011).
- [4] M. Devoret, S. Girvin, and R. Schoelkopf, *Ann. Phys.* **16**, 767 (2007).
- [5] A. A. Houck, J. A. Schreier, B. R. Johnson, J. M. Chow, J. Koch, J. M. Gambetta, D. I. Schuster, L. Frunzio, M. H. Devoret, S. M. Girvin, and R. J. Schoelkopf, *Phys. Rev. Lett.* **101**, 080502 (2008).
- [6] J. Bourassa, J. M. Gambetta, A. A. Abdumalikov, O. Astafiev, Y. Nakamura, and A. Blais, *Phys. Rev. A* **80**, 032109 (2009).
- [7] T. Niemczyk, F. Deppe, H. Huebl, E. P. Menzel, F. Hocke, M. J. Schwarz, J. J. Garcia-Ripoll, T. H. D. Zueco, E. Solano, A. Marx, and R. Gross, *Nature Physics* **6**, 772 (2010).
- [8] S. Filipp, M. Göppl, J. M. Fink, M. Baur, R. Bianchetti, L. Steffen, and A. Wallraff, *Phys. Rev. A* **83**, 063827 (2011).
- [9] O. Viehmann, J. von Delft, and F. Marquardt, *Phys. Rev. Lett.* **107**, 113602 (2011).
- [10] A. Cottet, *Implementation of a quantum bit in a superconducting circuit*, Ph.D. thesis, Université Paris VI (2002).
- [11] J. Koch, T. M. Yu, J. Gambetta, A. A. Houck, D. I. Schuster, J. Majer, A. Blais, M. H. Devoret, S. M. Girvin, and R. J. Schoelkopf, *Phys. Rev. A* **76**, 042319 (2007).
- [12] J. A. Schreier, A. A. Houck, J. Koch, D. I. Schuster, B. R. Johnson, J. M. Chow, J. M. Gambetta, J. Majer, L. Frunzio, M. H. Devoret, S. M. Girvin, and R. J. Schoelkopf, *Phys. Rev. B* **77**, 180502 (2008).
- [13] A. Blais, R.-S. Huang, A. Wallraff, S. M. Girvin, and R. J. Schoelkopf, *Phys. Rev. A* **69**, 062320 (2004).
- [14] E. Jaynes and F. Cummings, *Proceedings of the IEEE* **51**, 89 (1963); M. Tavis and F. W. Cummings, *Phys. Rev.* **170**, 379 (1968).
- [15] L. DiCarlo, J. M. Chow, J. M. Gambetta, L. S. Bishop, B. R. Johnson, D. I. Schuster, J. Majer, A. Blais, L. Frunzio, S. M. Girvin, and R. J. Schoelkopf, *Nature* **460** (2009), doi:10.1038/nature08121.
- [16] J. Bourassa and A. Blais, Private communication.
- [17] In current realizations of the 3D-transmon qubits, the length of the antenna is between 1 and 10% of the wavelength of the fundamental bare cavity mode.
- [18] M. D. Reed, L. DiCarlo, S. E. Nigg, L. Sun, L. Frunzio, S. M. Girvin, and R. J. Schoelkopf, *Nature* **482**, 382 (2012).
- [19] V. E. Manucharyan, E. Boaknin, M. Metcalfe, R. Vijay, I. Siddiqi, and M. Devoret, *Phys. Rev. B* **76**, 014524 (2007).
- [20] R. M. Foster, *Bell System Technical Journal* **3**, 260 (1924).
- [21] E. R. Beinger, R. H. Dicke, N. Marcuvitz, C. G. Montgomery, and E. M. Purcell, *Principles of Microwave Circuits*, edited by C. G. Montgomery, R. H. Dicke, and E. M. Purcell (MIT Radiation Laboratory, 1945).
- [22] The case of infinitely many discrete modes necessitates an extension of Foster's theorem as discussed in [29], but the results presented here still apply.
- [23] M. H. Devoret, "Quantum fluctuations in electrical circuits," (Elsevier Science B. V., 1995) Chap. 10, p. 351, les Houches, Session LXIII.
- [24] A. A. Clerk, M. H. Devoret, S. M. Girvin, F. Marquardt, and R. J. Schoelkopf, *Rev. Mod. Phys.* **82**, 1155 (2010).
- [25] M. Boissonneault, J. M. Gambetta, and A. Blais, *Phys. Rev. Lett.* **105**, 100504 (2010).
- [26] A. O. Caldeira and A. J. Leggett, *Phys. Rev. Lett.* **46**, 211 (1981).
- [27] See appended supplementary material.
- [28] K. Gloos, R. S. Poikolainen, and J. P. Pekola, *Applied Physics Letters* **77**, 2915 (2000).
- [29] M. K. Zinn, *Bell System Technical Journal* **31**, 378 (1951).
- [30] F. Pobel, *Matter and Methods at Low Temperatures*, 3rd ed. (Springer, 1937).
- [31] J. Krupka, K. Derzakowski, M. To-bar, J. Hartnett, and R. G. Geyer, *Measurement Science and Technology* **10**, 387 (1999).
- [32] Note that strictly speaking the commutator is rather $[\exp(i\varphi_s), n_s] = -\hbar \exp(i\varphi_s)$, but as we neglect charge dispersion, it is consistent to neglect the 2π -periodicity of the commutation relation.

Supplementary Material for “Black-box superconducting circuit quantization”

Simon E. Nigg, Hanhee Paik, Brian Vlastakis, Gerhard Kirchmair, Shyam Shankar
Luigi Frunzio, Michel Devoret, Robert Schoelkopf and Steven Girvin
Departments of Physics and Applied Physics, Yale University, New Haven, CT 06520, USA
(Dated: April 4, 2012)

These notes provide further details on the HFSS simulation of the cavity admittance used to build the effective low-energy Hamiltonian in the black-box quantization approach to compare with the single junction experiment and on the black-box quantization method for the multi-qubit case.

HFSS MODELING OF A 3D-TRANSMON

As discussed in the main text, the information about the spectrum of the quantum circuit, is encoded in the admittance at the port of the Josephson junction $Y(\omega) = Z(\omega)^{-1}$. More precisely, it is sufficient to know the real roots and the derivative of Y at these points.

Assuming that the size of the junction is negligibly small compared with the wavelength of the lower modes of the electromagnetic field in the cavity, it is appropriate to approximate the admittance of the linear part of the junction by a simple lumped element parallel LC oscillator with inductance L_J and capacitance C_J in parallel with the rest of the linear resonator. Hence the admittance can be decomposed as

$$Y(\omega) = j\omega C_J - \frac{j}{\omega L_J} + Y_c(\omega), \quad (10)$$

where $Y_c(\omega)$ is the admittance of the system without the junction. The latter quantity can in principle be directly measured but in this particular design a measurement is not practical. Instead we simulate the classical system *without* the junction by solving Maxwell’s equations numerically using HFSS. Fig. 3 shows a graphical representation of the different meshes used to represent the different elements of the cavity and antenna system. The smaller the element, the finer the mesh needs to be for accuracy and convergence. In this finite element simulation all metallic parts (Antenna and cavity boundaries made of pure aluminum), are treated as perfect conductors with zero resistance. In doing so, we neglect the kinetic inductance of the antenna and cavity. The finite London penetration depth of roughly $\lambda \approx 15$ nm would lead to an effective increase of the cavity size and hence a decrease of the cavity frequency of about 10 kHz. Furthermore, the kinetic inductance of the antenna and wire connecting the two antenna pads to the Josephson junction can be estimated as

$$L_k = \frac{\lambda\mu_0}{2 \tanh\left(\frac{d}{2\lambda}\right)} \left[\frac{L}{W} + \frac{l}{w} \right], \quad (11)$$

where $d \approx 100$ nm is the thickness of the aluminum layer, $L \approx 1$ mm is the total length and $W \approx 250$ μ m the width of the antenna and $l \approx 34$ μ m is the length and $w \approx 1$ μ m the width of the wire. With these numbers we obtain $L_k \approx 1.6 \cdot 10^{-3}$ nH, which is about three orders of magnitude smaller than (the linear part of) the Josephson inductance. A simple estimate shows that this would lead to a negative shift of the qubit resonance of only a few hundreds of kHz. These corrections are negligible at the current level of accuracy but can be easily included in the numerical simulation if necessary.

The aluminum antenna is evaporated on top of a sapphire substrate, the thickness of which is 430 μ m for samples 1, 2, 4 and 5 and 500 μ m for samples 3 and 6. The contraction of aluminum with decreasing temperature leading to a shrinkage of the cavity of about 0.5% and the reduction of the permittivity of sapphire by less than a per cent are taken into account [30, 31].

The imaginary and real parts of the resulting admittance Y are shown in Fig. 4 for $C_J = 0.34$ ff over a range of frequencies spanning three modes. The lowest mode with the largest slope is

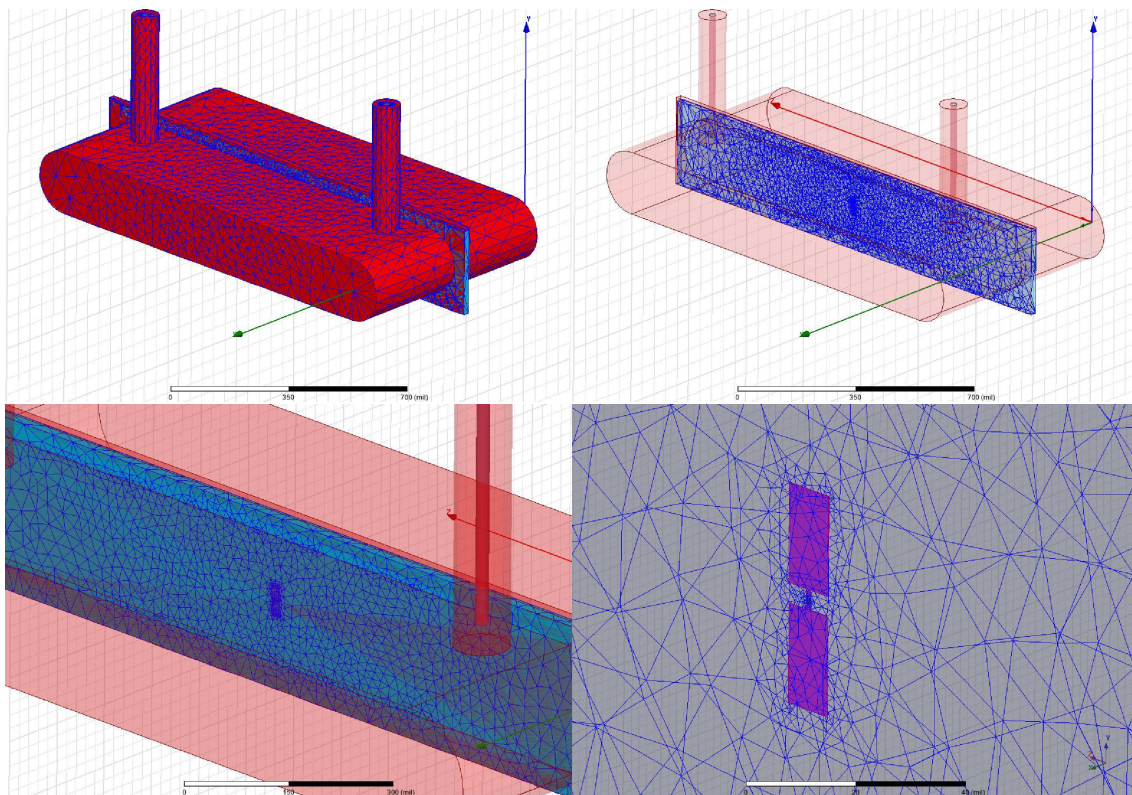


FIG. 3. (Color online) HFSS model of a 3D-transmon. (a) The 3D resonator with input and output ports. These are terminated by 50 Ohm ports. (b) Transparent view of the cavity showing the sapphire substrate. Because the electric field is concentrated in the dielectric, a finer mesh is used. (c) and (d) Zoom-ins on the antenna placed on top of the substrate. The mesh is finest around the antenna.

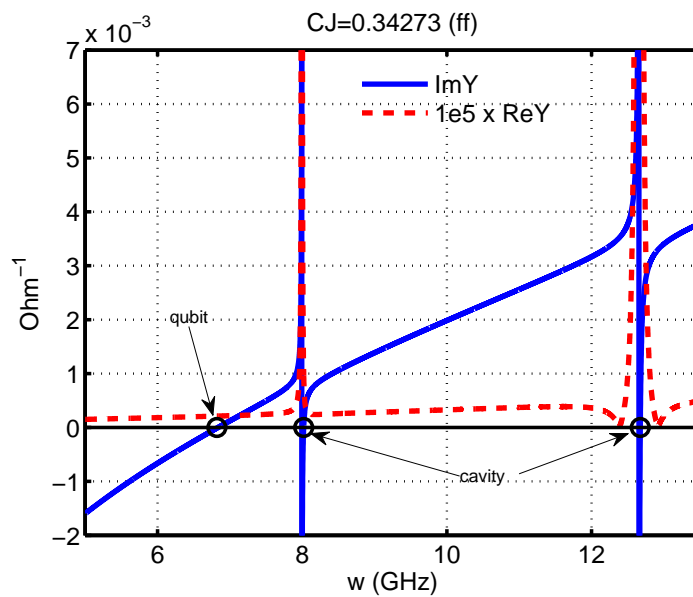


FIG. 4. (Color online) Real and imaginary parts of the admittance $Y(\omega) = j\omega C_J - \frac{j}{\omega L_J} + Y_c(\omega)$ as obtained from the HFSS simulation.

identified with the qubit mode and the remaining ones with cavity modes, although it must be kept in mind that the states corresponding to these modes are all superpositions of the bare modes. With this input, the corrections due to the nonlinearity of the junction are computed as explained in the main text. The results of the fit in C_J are given in Table I of the main text and plotted in Fig. 5. Details on the measurement of the spectrum can be found in Paik *et al.* [3].

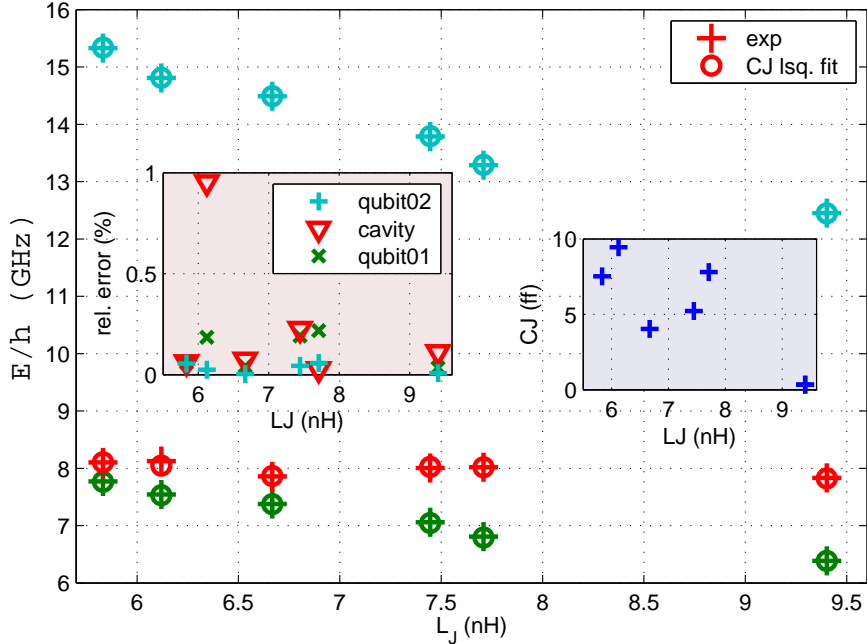


FIG. 5. (Color online) Low-energy spectrum of six 3D-transmons. Theory values (open circles) are obtained by fitting C_J for each data set (stars). The green symbols correspond to the $0 \rightarrow 1$ qubit transition, the red symbols to the lowest cavity resonance and the cyan symbols to the $0 \rightarrow 2$ qubit transition. The left inset show the sub % level relative errors between theory and experiment and the right inset shows the fitted values of C_J .

BLACK-BOX QUANTIZATION WITH MULTIPLE JUNCTIONS

For simplicity we focus on the dissipationless case. We consider a system with N Josephson junctions with *bare* Josephson energies $E_J^{(s)}$ and charging energies $E_C^{(s)}$, $s = 1, \dots, N$, in parallel with a common linear dissipationless but otherwise arbitrary electromagnetic resonator as depicted in Fig. 6 (a). The unbiased isolated junctions alone are described by the Hamiltonian $H_J = \sum_{s=1}^N \left(4E_C^{(s)} (n_s)^2 - E_J^{(s)} \cos(\varphi_s) \right)$, where n_s is the Cooper-pair number operator of the s -th junction conjugate to the phase degree of freedom φ_s , i.e. $[\varphi_s, n_s] = i\hbar$. [32] A corresponding N -port *linear* circuit, shown in Fig. 6 (b), is then defined by associating a port with each junction and replacing the latter with a parallel lumped element LC oscillator with inductance $L_J^{(s)} = (\phi_0)^2 / E_J^{(s)}$ and capacitance $C_J^{(s)} = e^2 / (2E_C^{(s)})$. Here and in the following $\phi_0 = \hbar / (2e)$ is the reduced flux quantum. This corresponds to expanding the cosines in H_J to second order in φ_s . We next consider this linearized circuit classically.

A quantity of central importance in the following is the N -port impedance matrix \mathbf{Z} with elements $Z_{ss'}(\omega) = V_s(\omega) / I_{s'}(\omega) \Big|_{I_i=0, i \neq s'}$. Let us choose arbitrarily one reference port k among the N ports. By virtue of Foster's theorem [20] $Z_{kk}(\omega)$ is a purely imaginary meromorphic function and can be synthesized by the equivalent circuit of parallel LC oscillators in series shown in Fig. 6 (c).

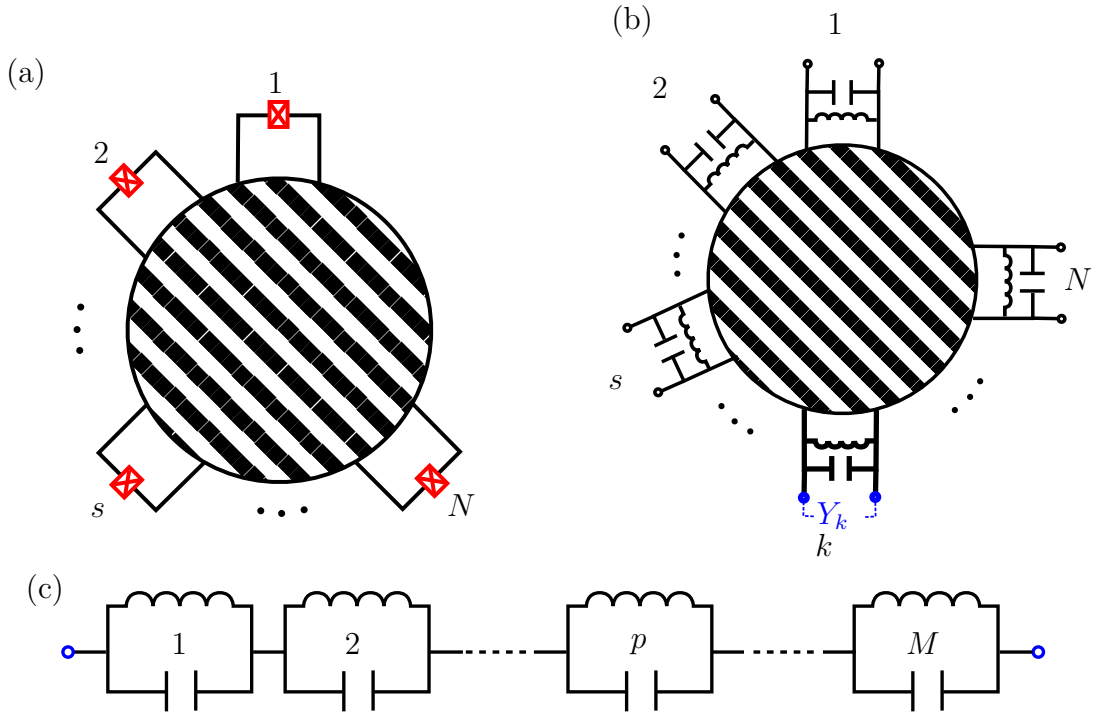


FIG. 6. (Color online) (a) Schematics of N JJs (gray (red) boxed crosses) coupled to an arbitrary linear circuit (striped disk). (b) Corresponding linearized N -port circuit with JJs replaced by parallel LC oscillators. (c) Foster-equivalent circuit of the impedance $Z_{kk}(\omega)$ of the linearized circuit shown in (b). The reference port $k \in \{1, \dots, N\}$ may be chosen arbitrarily.

Explicitly

$$Z_{kk}(\omega) = \sum_{p=1}^M \left(j\omega C_p^{(k)} + \frac{1}{j\omega L_p^{(k)}} \right)^{-1}, \quad (12)$$

where M is the number of modes and we have adopted the electrical engineering convention of writing the imaginary unit as $j = -i$. This equivalent circuit mapping corresponds, in electrical engineering language, to diagonalizing the linearized system of coupled harmonic oscillators. Accordingly, the eigen-frequencies $\omega_p = (L_p^{(k)} C_p^{(k)})^{-\frac{1}{2}}$ are determined by the poles of Z_{kk} or more conveniently by the real roots of the admittance defined as $Y_k = Z_{kk}^{-1}$ and the effective capacitances are determined by the frequency derivative on resonance of the latter as $C_p^{(k)} = (1/2)\text{Im}Y_k'(\omega_p)$. Note that [20] $\text{Im}Y_k'(\omega) > 0$. The Lagrangian of the system can be written as

$$\mathcal{L} = \frac{1}{2} \sum_{p=1}^M \left(C_p^{(k)} (\dot{\phi}_p^{(k)}(t))^2 + \frac{(\phi_p^{(k)}(t))^2}{L_p^{(k)}} \right),$$

in terms of the normal (flux) coordinates $\phi_p^{(k)}(t) = f_p^k e^{j\omega_p t} + (f_p^k)^* e^{-j\omega_p t}$, associated with each of the equivalent LC oscillators. From this, we can immediately write the Hamiltonian function of the equivalent circuit as $\mathcal{H}_0 = 2 \sum_{p=1}^M (f_p^k)^* (L_p^{(k)})^{-1} f_p^k$, where the subscript 0 indicates that we consider the linear circuit (Fig. 6 (b)). Note that the eigen-frequencies do not depend on the choice of port, while the eigenmodes do. Kirchhoff's voltage law implies that up to an arbitrary constant, $\varphi_k(t) = \phi_0^{-1} \sum_{p=1}^M \phi_p^{(k)}(t)$, where according to Josephson's second relation, $\varphi_k(t) = \phi_0^{-1} \int_{-\infty}^t V_k(\tau) d\tau$ is the phase variable of the k -th (reference) junction with voltage V_k . Importantly this simple relation holds only for the junction at the reference port k . In order to find the corresponding expressions for the other junctions ($s \neq k$), we notice that the AC voltage amplitude $V_s(\omega) = j\omega \phi_s^{(k)}(\omega)$ at

frequency ω generated across port s in response to a current with amplitude $I_{s'}(\omega)$ applied at port s' is given by $V_s(\omega) = Z_{ss'}(\omega)I_{s'}(\omega)$. Hence we have $\varphi_s^{(k)}(\omega) = (Z_{sk}(\omega)/Z_{kk}(\omega))\varphi_k(\omega)$. Combining this with the above we find that

$$\varphi_s^{(k)}(t) = \phi_0^{-1} \sum_{p=1}^M \frac{Z_{sk}(\omega_p)}{Z_{kk}(\omega_p)} (f_p^k e^{j\omega_p t} + (f_p^k)^* e^{-j\omega_p t}). \quad (13)$$

Quantization is achieved in the canonical way [23, 24] by replacing the flux amplitudes of the equivalent oscillators by operators as

$$f_p^{k(*)} \rightarrow \sqrt{\frac{\hbar}{2} \mathcal{Z}_{kp}^{\text{eff}}} a_p^{(\dagger)}, \quad \mathcal{Z}_{kp}^{\text{eff}} = \frac{2}{\omega_p \text{Im} Y_k'(\omega_p)}, \quad (14)$$

with the dimensionless bosonic annihilation (creation) operators a_p (a_p^\dagger). Direct substitution yields the Hamiltonian $H_0 = \sum_l \hbar \omega_l a_l^\dagger a_l$ of M uncoupled harmonic oscillators (omitting the zero point energies) and the Schrödinger operator of phase of the l -th junction is

$$\hat{\varphi}_s^{(k)} = \phi_0^{-1} \sum_{p=1}^M \frac{Z_{sk}(\omega_p)}{Z_{kk}(\omega_p)} \sqrt{\frac{\hbar}{2} \mathcal{Z}_{kp}^{\text{eff}}} (a_p + a_p^\dagger). \quad (15)$$

This is Eq. (7) of the main text using that $\hat{\varphi}_s^{(k)} = \phi_0 \hat{\varphi}_s$. The superscript makes explicit the dependence on the reference port. Accordingly the root mean square fluctuation of the flux of junction s in the multi-mode Fock state $|n_1, n_2, \dots, n_M\rangle$ is given by $\sqrt{\langle (\hat{\varphi}_s^{(k)})^2 \rangle} = \frac{\hbar}{2} \sum_{p=1}^M \left(\frac{Z_{sk}(\omega_p)}{Z_{kk}(\omega_p)} \right)^2 \mathcal{Z}_{kp}^{\text{eff}} (1 + 2n_p)$.

The anharmonic terms generated by the non-linearity of the Josephson inductance, necessary to build a qubit, are included by expressing the higher order terms in the expansion of the cosine in the harmonic basis. Including up to the quartic terms we obtain explicitly after normal ordering

$$H = H_0 - \sum_{pp'} \gamma_{pp'} \left(2a_p^\dagger a_{p'} + a_p^\dagger a_{p'}^\dagger + a_p a_{p'} \right) \quad (16)$$

$$- \sum_{pp'qq'} \beta_{pp'qq'} \left(6a_p^\dagger a_{p'}^\dagger a_q a_{q'} + 4a_p^\dagger a_{p'}^\dagger a_q^\dagger a_{q'} + 4a_p^\dagger a_{p'} a_q a_{q'} + a_p a_{p'} a_q a_{q'} + a_p^\dagger a_{p'}^\dagger a_q^\dagger a_{q'}^\dagger \right) + \sum_{s=1}^N \mathcal{O}(\hat{\varphi}_s^6),$$

with coefficients $\beta_{pp'qq'} = \sum_{s=1}^N \frac{e^2}{24L_j^{(s)}} \xi_{sp} \xi_{sp'} \xi_{sq} \xi_{sq'}$ and $\gamma_{pp'} = 6 \sum_{q=1}^M \beta_{qqpp'}$ where, choosing the first port as the reference port, $\xi_{sp} = \frac{Z_{s1}(\omega_p)}{Z_{11}(\omega_p)} \sqrt{\mathcal{Z}_{1p}^{\text{eff}}}$. Treating the φ^4 nonlinearity in first order perturbation theory, one obtains the expressions for the energy, generalized chi-shift and generalized anharmonicity given by Eq. (9) of the main text.